Morphological, Electrical, and Mechanical Characterization of Electrospun Nanofiber Mats Containing Multiwalled Carbon Nanotubes

Seth D. McCullen,[†,‡] Derrick R. Stevens,[§] Wesley A. Roberts,[§] Satyajeet S. Ojha,[†] Laura I. Clarke,[§] and Russell E. Gorga*[,†]

Fiber and Polymer Science Program, Department of Textile Engineering, Chemistry and Science, North Carolina State University; Joint Department of Biomedical Engineering, University of North Carolina at Chapel Hill and North Carolina State University; and Department of Physics, North Carolina State University, Raleigh, North Carolina 27695

Received July 31, 2006; Revised Manuscript Received December 14, 2006

ABSTRACT: This work focuses on the development of electrically conducting porous nanocomposite structures by the incorporation of multiwalled carbon nanotubes (MWNT) into electrospun poly(ethylene oxide) (PEO) nanofibers. Electron microscopy confirmed the presence of individual aligned MWNT encapsulated within the fibers and showed fiber morphologies with diameters of 100−200 nm. Electrical conductance measurements of the random nanofiber mats showed that by increasing the concentration of MWNT we were able to produce porous nanocomposite structures with dramatically improved electrical conductivity. Above a percolation threshold of 0.365 ± 0.09 MWNT weight percent (wt %) in PEO the conductance increased by a factor of 10^{12} and then became approximately constant as the concentration of MWNT was further increased. Because of this percolation threshold, for a 1 wt % loading of MWNT, the conductivity is essentially maximized. Mechanical testing confirmed that the tensile strength did not change, and there was a 3-fold increase in the Young's modulus when comparing a 1 wt % MWNT loading to the pure electrospun PEO. Thus, the optimal MWNT concentration for PEO nanofiber mats with enhanced mechanical and electrical properties is ∼1 wt %.

Introduction

Nanocomposites are materials that have the propensity to exhibit astonishing physical and electrical properties due to the interaction between the matrix and filler. Much work has focused on the implementation of carbon nanotubes as a filler in polymer matrices, and some success has been achieved at determining the physical properties of these systems.[1−4] The goal of this work is to create and characterize novel nanocomposites, in particular random mats of electrospun nanofibers, to be used as a model in creating functional substrates for a variety of applications ranging from electrical sensors to matrices for tissue engineering. Therefore, characterization of the overall mechanical and electrical properties of the random fibrous mat is essential to quantify the functionality of these structures. Specifically, this report focuses on the fabrication and electric and mechanical characterization of electrospun carbon nanotube/poly(ethylene oxide) (PEO) nanocomposites. Through this investigation, we will have a better representation of the nanocomposite characteristics by measuring the macroscopic nonwoven substrate, not just an individual fiber within the composite. Therefore, the properties measured here will be indicative of those of the composite in an application. A specific focus is on conductance measurements to delineate the parameters that determine the resultant conductivity of the isotropic fibrous mats, as electrical conductivity is important for both sensor and biomedical applications. Electron microscopy is utilized to determine fiber morphology and the orientation of the multiwalled carbon nanotubes (MWNT) within the fiber. A final consideration is the mechanical properties of the system with a goal of simultaneously optimizing the mechanical and electrical properties of random fibrous mats.

Carbon nanotubes are graphitic sheets rolled into seamless tubes (i.e., arrangements of carbon hexagons into tubelike fullerenes) and have diameters ranging from about a nanometer to tens of nanometers with lengths up to centimeters. Nanotubes have received much attention due to their interesting properties (high modulus and electrical/thermal conductivity) since their discovery by Iijima in 1991.[5,6] Since then, significant effort has gone into fabricating polymer/nanotube composites for improved strength and conductivity.[7−22] In general, for improved mechanical properties, the interaction between the filler material and polymeric matrix is the key to sustaining a compatible interface through the adhesive contact of the two materials.[23,24] When a conductive composite is desired, the most important parameter besides the apparent conductivity of the filler is the geometric shape; in particular, it is most advantageous to utilize fillers with an aspect ratio (length/diameter) greater than 1. Cylindrical materials such as carbon nanotubes exhibit this large aspect ratio, in the range of thousands, which alleviates the processing of the nanocomposite by assuring that only a low mass fraction is needed to obtain large increases in physical properties. Thus, carbon nanotubes are ideal candidates for nanocomposite applications and have demonstrated large increases in physical properties with relatively low mass fractions.

Here, electrospinning was used to fabricate nanocomposites constructed of carbon nanotube−polymer nanofibers. Electrospinning provides a means to construct a three-dimensional matrix by creating fibers with diameters on the nano- to microscale. The fibers are created by electrostatic repulsion and the Coulombic forces due to an external electric field applied to a polymer solution.[25,26] By applying a critical voltage between the metallic needle of a syringe filled with polymer solution

* Corresponding author: e-mail regorga@ncsu.edu, Fax 919-515-6532.
† Department of Textile Engineering, Chemistry and Science.
‡ Joint Department of Biomedical Engineering.
§ Department of Physics.

10.1021/ma061735c CCC: $37.00
Published on Web 01/25/2007

and a grounded collector, a polymer jet is generated which creates fibers that can be collected at the grounded plate.[25,27,28] The end result is a randomly oriented mat of fibers with a high porosity due to the high ratio of surface area to volume. This aspect of electrospun fibers is advantageous for use as a means of production for nanocomposites by generating an intimate level of interaction between the matrix and the filler due to both being on similar size scales.

Previous work on fibrous nanocomposites has highlighted the need for adequate dispersion of the filler in the matrix for enhanced mechanical properties.[4,21,22] Past research has shown that dispersion and orientation of the carbon nanotubes within a nanocomposite improves physical properties.[4,21,22] However, most of this work has utilized traditional polymer processing techniques such as melt-blending and coagulation spinning to name a few.[4] Dror et al. dispersed carbon nanotubes with the additive gum arabic to create a colloidal suspension of carbon nanotubes in solution prior to electrospinning and achieved a high level of carbon nanotube orientation within the nanofibers.[29] Here we utilize the Dror technique to form nanofibers with ~100 nm diameters.

Researchers who have explored the interaction of carbon nanotubes in electrospun matrices have documented differing conclusions.[29−33] This can be attributed to the polymeric system, the orientation, and the dispersion of the carbon nanotubes in the system in addition to the size scale of the carbon nanotubes, the diameter, and the length with respect to the matrix.[1] With respect to electrical properties of composite fibers, Sundaray was able to show an increase of 10 orders of magnitude in conductivity between 0 and 2 wt % carbon nanotube loading in single electrospun fiber.[33] However, this work did not display evidence of a percolation threshold between 0.05 and 2 wt %, and the authors hypothesized that, if present, the threshold was much lower than 0.05 wt %. Through this work, our aim is to produce electrospun nanocomposites containing varying mass fractions of carbon nanotubes to determine whether the conductance of the nonwoven mat (not the individual fiber) follows a percolation model and to report the percolation threshold via thorough conductance measurements. Again, it is essential to quantify the properties of the random fibrous mat to determine how the material behaves in bulk.

All measurements in this work were conducted on samples consisting of random nanofiber mats produced from electrospinning. By utilizing planar interdigitated electrodes onto which the mat can be directly electrospun, we can measure these extremely porous mats in their native state without concern of pinhole defects which can occur in a "sandwich" electrode configuration. In summary, we propose to optimize the parameters for the electrospinning process of PEO/carbon nanotube solutions, to determine whether the conductance exhibits percolative behavior, and to measure the tensile properties of electrospun fibrous mats.

Experimental Section

Materials and Nanocomposite Fabrication. PEO of M_w 400 000 was purchased from Scientific Polymer Products. Different wt % solutions were produced with deionized water. MWNT were supplied by Nano-Lab. The MWNT were produced by plasma-enhanced chemical vapor deposition using acetylene and ammonia with an iron catalyst and grown on a mesoporous silica substrate.[34] The MWNT used had a diameter of 15 ± 5 nm and length of 5−20 μm at 95% purity. The MWNT were dispersed using an Ultrasonic model 2000U generator and probe operating at 25 Hz. Varying masses of MWNT were added to 50 mL of deionized water and the dispersing agent gum arabic at a concentration of 3% and sonicated for 1 h. The sonicated solutions of MWNT and PEO in deionized water were combined and mixed by stirring. The solution was inspected optically for up to 30 days. Solutions containing gum arabic exhibited homogeneous suspensions through the 30 day period, whereas the nanotubes in solutions without gum arabic immediately fell out of suspension after sonication. The final solutions produced contained varying concentrations of MWNT from 0 to 3 wt % in 4 wt % PEO solution. No further processing occurred before electrospinning.

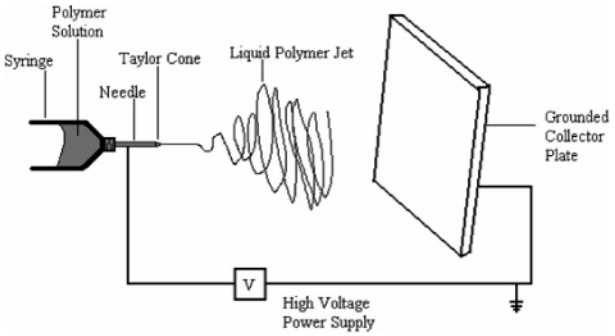

Figure 1. Schematic of the electrospinning apparatus used to produce the nanocomposite samples. Each component is labeled.

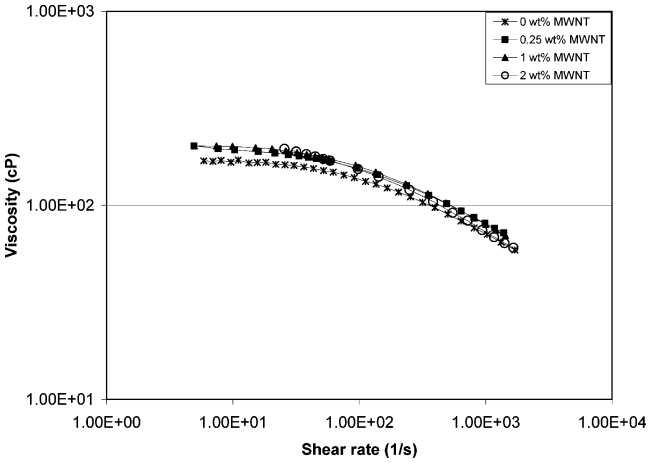

Figure 2. Flow curve plot of viscosity vs shear rate for MWNT/PEO solutions.

The electrospinning apparatus included a syringe pump obtained from New Era Pump Systems (model NE 500), which operated at a flow rate of 5−55 μL/min. The high-voltage power supply was obtained from Glassman (High Voltage model FC60R2 with a positive polarity). The operating voltage varied from 10 to 20 kV with an optimum electric field of 1 kV/cm. The solutions were loaded into 10 mL syringes with luer-lock connections and used in conjunction with a 4 in. 20 gauge blunt tip needle. The design of the electrospinning setup was based on a point-plate configuration, as can be seen in Figure 1.

The fibers were collected on either a plate or a pair of aligned collector bars. The plate produced a random nonwoven array, whereas the collector bars produced oriented fibers along the same axis between the bars. The electrospun mats were deposited onto aluminum foil, which was placed over the collector plate. For scanning electron microscopy (SEM) and mechanical testing, the samples were removed from the collector. For transmission electron microscopy (TEM) and conductance testing, samples were deposited directly onto TEM grids and microelectrodes, respectively.

Electrospun Nanocomposite Characterization. Rheological measurements were performed on the MWNT/PEO solutions using a StressTech HR rheometer with Reologica Instruments and ATS Systems. These experiments were performed using a parallel plate configuration for all measurements.

For SEM, a JEOL JSM-6400 FE w/ EDS, operating at 5 kV, was used to determine fiber morphology of the electrospun samples.

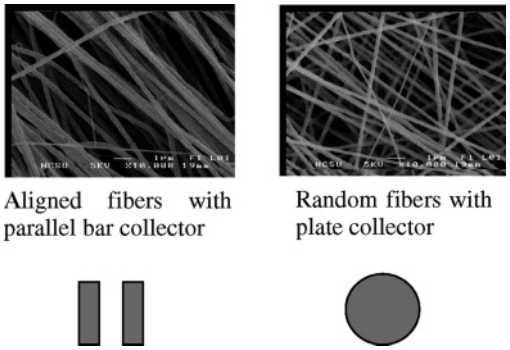

Figure 3. SEM of aligned and random nanofibers (1 wt % MWNT in 4 wt % PEO). Images were captured at 10 000×. The scale bar is 1 μm.

The electrospun samples were coated by a K-550X sputter coater with Au/Pd ~100 Å thick to reduce charging. Digital images were captured and analyzed using Scion Image software. TEM was performed on a JEOL 100S with samples spun directly on a Cu 400 mesh grid coated with holey thin carbon film. Micrographs were developed, digitally scanned, and not further modified.

Electrical measurements were performed on a Keithley model 6430 sub-femtoamp remote source meter. In order to easily measure the thin, porous matrix of nanofibers, flat interdigitated electrodes on glass were utilized for conductance measurements. Each electrode consisted of 26 finger pairs with 1 mm long, 10 μm wide digits spaced by 10 μm, and two contact pads of ~1 mm^2 each. Conductive silver epoxy connected the contact pads to external wires. Electrodes were fabricated using lift-off standard UV lithography on glass substrates followed by thermal evaporations of ~150 Å of chromium and 1150 Å of gold. Homemade triaxial cables connected the sample, which rested on a copper stage, to the remote source meter. The sample space was evacuated to ~1 × 10^{-7} Torr. Each electrode was measured before and after sample deposition, nominally from −10 to 10 V with 0.1 V steps and a 15 s wait after the application of a voltage change. For highly conductive samples, the voltage range was reduced. Samples were prepared by electrospinning a solution with known concentration of multiwalled carbon nanotubes, utilizing the same preparation conditions for each sample to obtain comparable thickness. Conductance values were obtained by fitting a line to the low-voltage linear region of the current−voltage characteristic. The fringe fields from interdigitated electrodes are known to penetrate into a film a distance roughly equivalent to the spacing between the digits. From the measured thickness of the mat as 1−3 μm, we expect some response from the fringing fields.[35] Consequently, the geometrical parameters needed to calculate the conductivity will be slightly altered. Furthermore, the extreme porosity of the nanocomposite mat makes a clear determination of the polymer density difficult. Thus, as a matter of convenience, we report conductance results only. A calibration to correct for the fringing fields is underway in our laboratory and will be reported in a future publication.

Mechanical properties were tested using an Instron model 5544 using the Bluehill version 1.00 software. Samples were prepared according to ASTM standard D4762-04. Each sample tested up to seven specimens with a sample width of 2 cm and a gauge length of 2.54 cm. The testing rate was ~25.4 cm/min. Samples were tested within 24 h of fabrication.

The volume of voids in the random fibrous mats was calculated using Image J analyzer. Images obtained by SEM were scanned through Image J. Different layers of nanofibers were made distinct a using grayscale. The area (proportional to volume) of nanofibers present in one plane was then calculated, and therefore void fraction was calculated in a single layer. This procedure was repeated four times for each sample for statistical purposes.

Results and Discussion

The viscosity of the spinning solution is essential for being able to produce a continuous flowing stream of polymer from the needle to the collector. Rheology measurements were performed to determine the effect on viscosity associated with an increase of MWNT and to verify whether the solutions were "spinnable". By understanding the rheological behavior of the solution, we are better able to control the processing parameters such as the flow rate. When analyzing the viscosity vs shear rate data (as shown in Figure 2), the polymer solution with suspended nanotubes behaved as a classical pseudo-plastic material, exhibiting shear-thinning behavior at increasing shear rates. With the addition of MWNT to the polymer solutions, there was a slight increase in the viscosity. This can be attributed to an increased turbidity of the solution due to the presence of the MWNT.

The flow of material during electrospinning is determined using the equation $Q = \Delta P/R$, where Q is the flow rate, ΔP is the pressure difference, and R is the resistance, equal to $8\eta L/$

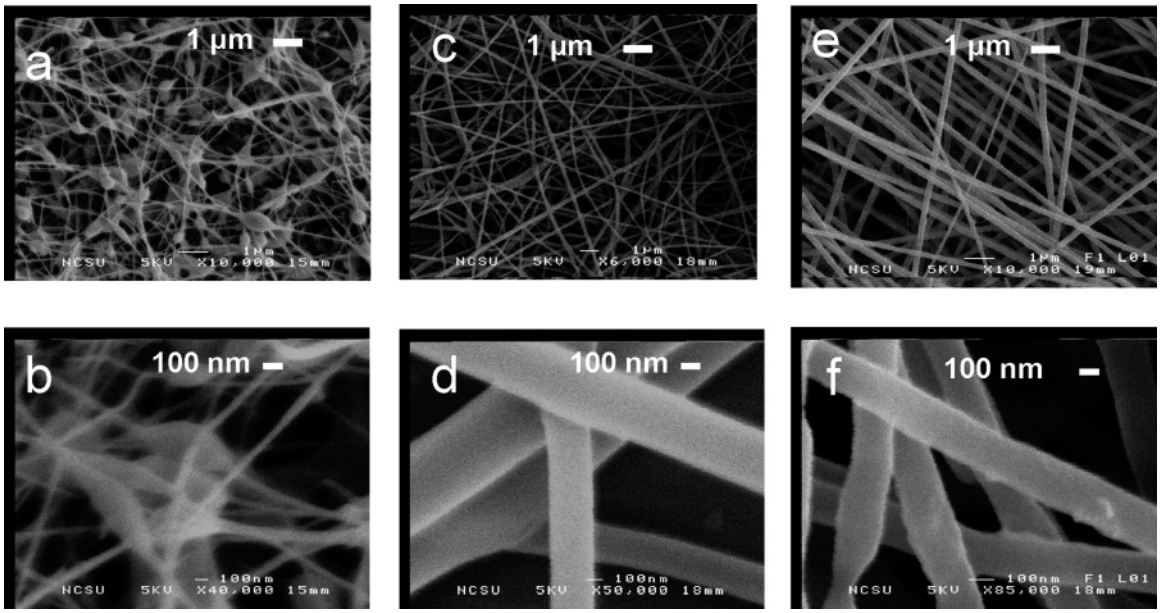

Figure 4. (a−f) SEM images of electrospun nanocomposites: (a, b) images of 3 wt % PEO, (c, d) images of 4 wt % PEO, (e, f) images of 4 wt % PEO with 1 wt % MWNT. By increasing the polymer concentration by 1%, uniform nanofibers were produced.

πr^4. For this equation L is the length of the capillary, r is the radius of the capillary, and η is the viscosity of the polymer solution. In order to determine the viscosity experienced during fiber formation, we can calculate the shear rate (Ψ) of our system with the following equation: $\Psi = 4Q/\pi R^4$.[36] For the operational conditions, we produced a shear rate within the lower region of the viscosity plot, which depended on the flow rate from the syringe pump. The flow rate ranged from 5 to 55 μL/min. For this electrospinning system, the shear rate is below 20 s^{-1}. When viewing the flow curve, we can easily observe that no shear thinning is occurring at this range. The effects of interfacial bond strength, particle size, and shape distribution can be analyzed from the strain dependence of dispersions. For this system the particles in solution are the MWNT. When these particles are dispersed, each individual MWNT is separated from other MWNT and no aggregates are present. Smaller particles and stronger interfacial bonds will increase the low strain modulus of a dispersion with a given particle concentration. Forces acting on the particle in solution include gravity and random thermal (Brownian) fluctuations. In Figure 2, the viscosity plots for the different suspensions of MWNT in PEO show that the samples are within the same range and that the MWNT do not significantly increase the viscosity of the solution. Thus, Figure 2 displays that the viscosity of PEO behaves similarly even with the addition of low mass fractions of MWNT. Also, the addition of MWNT does not change the shape of the flow curve for this polymer.

Orientation of the nanofibers can be controlled by the collector geometry. The plate collector morphology shows random orientation in all directions. Parallel bar collectors are able to align the nanofibers between the two collectors (as shown in Figure 3).

The polymer concentration can be viewed as a critical component that controls the morphology of the fibers produced. It was determined that less than 4 wt % PEO without MWNT produced beaded nanofibers. These structures exhibit poor mechanical properties due to their heterogeneous nature. By increasing the weight percent of our polymer to 4 wt %, fibers were produced without any bead formation. Figure 4 illustrates the difference in morphologies for differing weight percent concentrations. Incorporating the MWNT in a solution of 4 wt % PEO allows fabrication of uniform fibers with similar diameters. In contrast, spinning on the glass substrate of the interdigitated electrodes resulted in slightly beaded nanofibers for all MWNT concentrations. This can be attributed to the microelectrode not being completely grounded due to inadequate connection between the collector plate and the microelectrode front surface of the glass substrate. As beading in the nanofiber might be expected to decrease the conductance and increase the critical weight percentage, the electric conductance results can be considered upper and lower limits, respectively, on these quantities.

In order to quantify that the produced fibers did contain oriented MWNT, TEM was utilized to view the alignment and orientation of MWNT within the nanofibers produced. The arrangement of the nanotubes within the fibers is able to influence the behavior of the composite when testing for conductivity and mechanical properties. If the MWNT have a high orientation within the fibers, then the apparent properties of the nanotubes should become superimposed within the electrospun fibers. Figure 5 confirms that the MWNT are aligned along the fiber axis via the flow and electric field direction. In some instances it can be seen that more than one MWNT was encapsulated within the produced nanofibers. When more than one MWNT was encapsulated, a misshaped (or branched) nanofiber was produced, as shown in Figure 5b. However, these fibers show numerous MWNT all dispersed and oriented along the axis of numerous fibers bonded together. Bonding of the fibers could have taken place due to the solvent evaporating too slowly, connecting the fibers together.

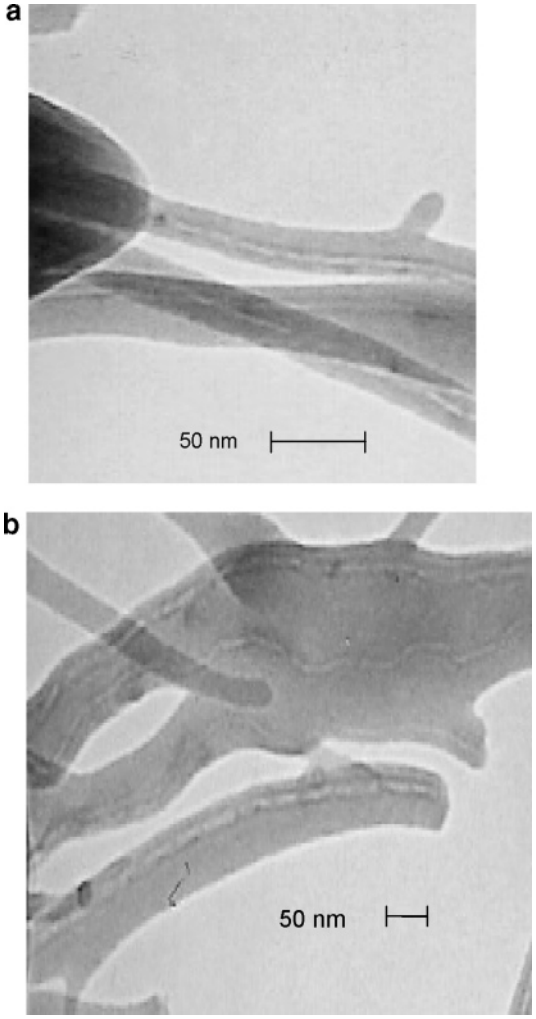

Figure 5. (a) TEM image of 2 wt % MWNT in 4 wt % PEO nanofibers showing dispersion and alignment along the axis of the fiber. (b) TEM image of 2 wt % MWNT in 4 wt % PEO sample. This image captures four multiwalled carbon nanotubes within several nanofibers bonded together.

For composite systems composed of a conducting filler (MWNT) embedded in an insulating matrix (PEO), classical percolation theory is often invoked.[37] In short, the system is described as randomly orientated and positioned conducting rods in an insulating background. As the concentration of the conducting element is increased, conduction occurs when the density of MWNT is sufficient to create a single percolating path across the sample.[37] Below this critical concentration, any conductance is due to the polymer matrix and independent of MWNT concentration. As the density of filler further increases above the threshold value, the conductivity dramatically increases as more and more paths contribute to the current. Once current is flowing throughout the full geometrical volume of the sample, further increase in MWNT concentration has little effect and the conductance plateaus with only a slight dependence on nanotube density.[37] It is important to note that several of the assumptions implicit in classical percolation theory are not maintained in the electrospun MWNT/PEO system.[38−40] As shown above, the embedded nanotubes are generally aligned

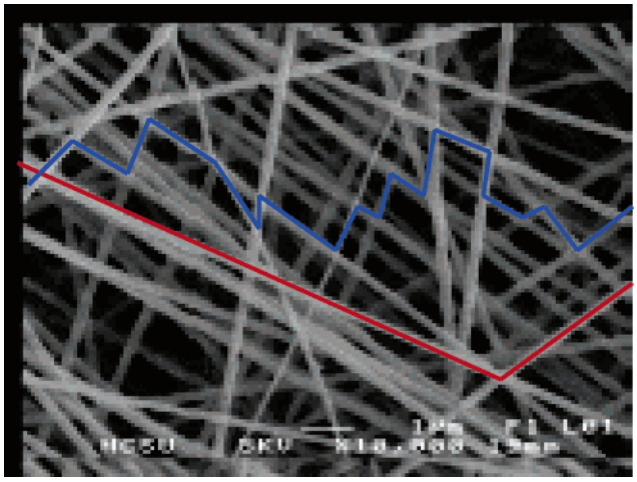

Figure 6. Two hypothetical routes for percolation along fibers and their intersections. The distance across the micrograph is comparable to the spacing of the electrode (~12 μm).

along the fiber axis, rather than being randomly oriented.[41−45] In addition, because the polymer and nanotubes are innately entangled, it is unlikely that true percolating paths, where all MWNT along the path are in physical contact, are formed and more likely that tunneling or hopping between MWNT plays a role in conduction.[38,46,47] Percolation theory has been extensively and successfully used to describe nanocomposite conductivity, and as shown below, our results also indicate a percolation effect.

In this research the composite is formed of three elements: conducting nanotubes, polymer (nonconducting), and open space or voids. The morphological characteristics of both the fiber and the resulting mat may strongly influence the nature of the percolation process and the ultimate conductance of the material. For instance, significant MWNT alignment is observed in these fibers under SEM imaging, which may alter the critical weight percentage from that of an isotropic distribution.[42] If such alignment is a function of fiber diameter, changing the fiber size may affect the percolation threshold of the system. When combining the fibers into the technologically important structure of a mat, additional variables such as mat density (the fraction of void space), the number of fiber intersections, and the character of these fiber−fiber contacts come into play. For instance, even if MWNT density is below that needed to carry current along long lengths of fiber, a mat may produce a percolating path consisting of short sections of several different fibers (blue path in Figure 6) if there is a sufficiently high density of fiber−fiber connections. The shorter blue lines represent portions of individual MWNT within a fiber, and the path is formed from connections between fibers. This would lead to a lower percolation threshold in the mat than for the fiber alone. In contrast, if fiber−fiber intersections are weak (leading to poor contacts between nanotubes) or if the fibers are aligned in the mat and rarely cross, the current may be carried predominantly along individual fibers (red path in Figure 6). In each red line, multiple nanotubes within the fiber overlap to form a long conducting path along the fiber. Here the percolation threshold of the mat might be similar to that of the fiber.

Thus, rather than generating universal values for the critical doping of MWNT in PEO nanofibers, we expect that our results are specific to the degree of nanotube alignment, the interface between the polymer and nanotube, the fiber size, the morphology of the mat, and the contact between fibers therein. This research represents a specific example of a conducting mat and an attempt to begin understanding the relative importance of these morphological factors.

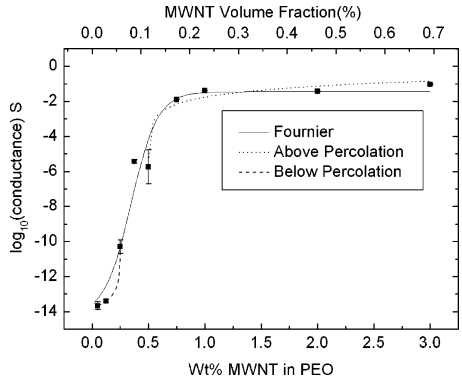

Figure 7. Electrical conductance vs MWNT concentration in 4 wt % PEO or, alternatively, vs the measured volume fraction of MWNT. With increasing MWNT concentration, the conductance demonstrates a percolation threshold for the random mats. The three fits are described in the text, with fit parameters presented in Table 1.

We point out that an alterative model for this system can be obtained from work on doping polymer blends where the dopant resides primarily in one polymer type and a second material (in our case void space) takes up the remaining volume.[48−51] In these polymer blend studies, a so-called double-percolation process (reflecting the dependence on both doping density and percentage of volume-excluding polymer) is predicted. As discussed below, in this work, we do not alter the fraction of void space in our mats and observe percolation as a function of doping at this one value.

Using the techniques previously described, current−voltage characteristics of PEO with varying MWNT concentrations were recorded. A background, the current−voltage characteristic of each bare electrode, was taken before all depositions. All blank electrodes showed similar curves with a measured conductance of 6.3×10^{-15} S, which serves as the lower limit of our measurement range. With the addition of MWNT to the PEO solution, the conductance vs MWNT concentration curve showed a dramatic increase consistent with a percolating behavior, as seen in Figure 7. Figure 7 shows the conductance data plotted against two axes: the variable controlled in the experiment (the weight percent of MWNT in the PEO solution) or, alternatively, the experimentally observed volume fraction of MWNT. In the latter approach, the top layer of an SEM image of mats at 0 and 1 wt % MWNT was analyzed to determine the fraction of fiber and void space. Taking an average of four measurements for each image, the void space represented 74.79 $\pm$ 2% and 74.85 $\pm$ 2% for pure PEO and 1 wt % MWNT, respectively. On the basis of these measurements, we conclude that the void space is constant over the nanotube doping range used in this work. Because the void and polymer are both insulating, the system is modeled as conducting MWNT embedded in this combined matrix. On the basis of the known doping, the fraction of MWNT to total volume is calculated. We observed that small variations in sample preparation, including dispersion of the MWNT in solution, can introduce significant changes in the resulting conductance. This can account for the 0.5 wt % sample having a slightly lower conductance than the 0.35 wt %. The placement of these points did not affect our overall results.

Figure 7 generates two alternative two-component systems to study. A model that ignores the void space and focuses on the density of MWNT in the PEO, minimizes the effect of the mat morphology, and assumes that most conduction is along

Table 1. Parameters for the Three Conductance Fits Models Used[a]

Fournier		above percolation		below percolation	
G_n	0.036 ± 0.04 S	a'	0.043 ± 0.02 S	c'	$2.3 \times 10^{-15} \pm 4 \times 10^{-15}$ S
G_m	6.3×10^{-15} S[a]	t	1.3 ± 0.6	s	1.4 ± 0.7
b	8.5 ± 1.8	p_c	0.45 ± 0.01	p_c	0.25 ± 0.04
p_c	0.35 ± 0.04				

[a] G_m was held at the conductance limit of our system. G_n, G_m, a', and c' are the conductance equivalents of the conductivity quantities given in the text.

the fibers. Alternatively, modeling the nanotube density in the entire volume (voids + polymer) assumes the system is similar to randomly doped, homogeneous film of the combined matrix (voids + polymer). Clearly, the true physical situation is between these two extremes.

We characterize the conductance vs MWNT concentration curves with three alternative fits. Here we focus on the experimentally controlled variable, the MWNT weight precent; equivalent volume fraction values can be obtained by scaling according to Figure 7. The data is best represented by the Fournier model: $\log(\sigma) = \log(\sigma_n) + [\log(\sigma_m) - \log(\sigma_n)]/(1 + \exp[b(p - p_c)])$ which fits points above, below, and throughout the percolation threshold region.[52,53] Here, σ, σ_n, and σ_m are the composite, nanotube, and polymer conductivity, respectively. MWNT concentration is represented by p, with p_c the critical weight percentage to obtain percolation. The empirical parameter b directs the change in conductance across the threshold. Data above the percolation threshold were also fit with $\sigma = a(p - p_c)^t$ from classical percolation theory. Data below the threshold can be fit with a similar functional form: $\sigma = c(p_c - p)^{-s}$.[47] In these cases, a, c, s, and t are fit parameters. Because conductance $G \propto \sigma$, with a proportionality constant that depends only on the geometry of the sample, p_c, b, t, and s should be unaffected by fitting conductance (rather than conductivity) data.

The fits and parameters can be seen in Figure 7 and Table 1. While the Fournier form yields the best fit to the data, all three fits give similar percolation thresholds of 0.35 ± 0.04, 0.50 ± 0.01, and 0.25 ± 0.04 wt % MWNT, respectively. These values are higher than the percolation threshold of <0.05 wt % MWNT observed for a single composite fiber of larger diameter (diameter 200 nm−6 μm) from poly(methyl methacrylate).[33] We find an exponent value of 1.32 ± 0.6 for t, which is slightly lower than the standard values of 1.7−2.0 for 3-D systems[54] and consistent with the expected value (1.3) for 2-D arrays.[55,56] Work on other carbon-filled three-dimensional systems has reported a wide range of t values, including similar low exponents.[47,54,57−59] Nevertheless, the observation of an exponent with reduced dimensionality may reflect the influence of the fiber geometry on the percolation;[60] in particular, polymer blend systems where the dopant is constrained to the interface between the polymers have shown similar results.[57,61,62] We find a value of $s = 1.39 \pm 0.7$, which is greater than the expected value of ~0.7−0.9 in 3-D and consistent with $s = 1.3$ in 2-D.[47,61,63] Finally, recent studies linked composite systems with $t > 2$ to tunneling between conductive elements due to an intermediate insulating layer (poor constant between doping elements).[54,64] Our value of t indicates no evidence of this effect.

To determine any changes in mechanical properties due to MWNT concentrations, tensile tests were performed on MWNT loading levels of 0, 1, and 3 wt %. For each sample measured, the thickness was determined by the mean of 10 measurements per sample. Each sample was collected from the plate collector and removed from the aluminum foil. The samples analyzed included a pure 4 wt % PEO sample, 1 wt % MWNT/4 wt % PEO, and 3 wt % MWNT/4 wt % PEO. The results are shown in Table 2. The stress calculation accounts for the void volume fraction (75%), which was determined to be independent of MWNT concentration (as discussed earlier). With the addition of MWNT, both the 1 and 3% samples demonstrated a statistically significant reduction in elongation. The 1 wt % MWNT/PEO sample maintained the same tensile stress yet had a statistically significant increase in modulus when compared to the pure PEO sample. However, the 3 wt % MWNT/PEO sample demonstrated a reduction in tensile stress with no change in modulus as compared to the pure PEO sample. This can be attributed to agglomeration of MWNT at the higher concentration, which could act as stress concentrations, leading to premature breaking.

Table 2. Modulus and Tensile Strength as a Function of Nanotube Concentration

sample	modulus (MPa)	tensile strength (MPa)
0% MWNT	12.28 ± 1.54	9.96 ± 0.20
1% MWNT	37.68 ± 2.14	9.40 ± 0.36
3% MWNT	23.56 ± 1.67	5.04 ± 0.25

Conclusions

This work demonstrates the fabrication, determination of optimal process parameters, and mechanical and electrical characterization of 100−200 nm PEO nanofibers with dispersed, encapsulated MWNT. Rheology measurements confirmed that the nanotubes were well-dispersed and integrated within the polymer solution used for electrospinning and that the viscosity, and thus flow curve of the polymer, was not significantly altered by the addition of low concentration of MWNT. This indicates that the electrospinning parameters are robust in this concentration regime. Randomly oriented, isotropic mats of the nanofibers were generated by utilizing a plate collector. A 4% or greater PEO solution in deionized water was required for the formation of uniform diameter fibers. Conductance measurements on random mats showed a percolation threshold at ~0.35 wt % MWNT, depending on the model used for fitting. Above, about 1 wt %, the conductivity was maximized. Mechanical testing of the random mats showed an optimal Young's modulus also at the value of 1 wt % MWNT, indicating that this loading value is optimal for maximizing both mechanical and electrical properties.

Acknowledgment. This work was funded by the Nanotechnology Initiative at NC State University. W.A.R. acknowledges an Undergraduate Research Award from NC State. We especially thank Alfred Inman and Dr. Nancy Monteiro-Riviere for their time and assistance with electron microscopy. We also thank Dr. Wendy Krause for use of her rheometer and Rebecca Klossner and Kelly Stano for their technical assistance.

References and Notes

(1) Andrews, R.; Weisenberger, M. C. *Curr. Opin. Solid State Mater. Sci.* **2004**, *8*, 31−37.
(2) Harris, P. J. F. *Int. Mater. Rev.* **2004**, *49*, 31−43.
(3) Hussain, F.; Hojjati, M.; Okamot, M.; Gorga, R. E. *J. Compos. Mater.* **2006**, *40*, 1511−1575.
(4) Moniruzzaman, M.; Winey, K. I. *Macromolecules* **2006**, *39*, 5194−5205.
(5) Iijima, S. *Science* **1991**, *354*, 56−58.
(6) Iijima, S.; Ichihashi, T. *Nature (London)* **1993**, *363*, 603−605.

(7) Schadler, L. S.; Giannaris, S. C.; Ajayan, P. M. *Appl. Phys. Lett.* **1998**, *73*, 3842−3844.
(8) Haggenmueller, R.; Gommans, H. H.; Rinzler, A. G.; Fischer, J. E.; Winey, K. I. *Chem. Phys. Lett.* **2000**, *330*, 219−225.
(9) Qian, D.; Dickey, E. C.; Andrews, R.; Rantell, T. *Appl. Phys. Lett.* **2000**, *76*, 2868−2870.
(10) Lozano, K.; Bonilla-Rios, J.; Barrera, E. V. *J. Appl. Polym. Sci.* **2001**, *80*, 1162−1172.
(11) Lozano, K.; Barrera, E. V. *J. Appl. Polym. Sci.* **2000**, *79*, 125−133.
(12) Jin, L.; Bower, C.; Zhou, O. *Appl. Phys. Lett.* **1998**, *73*, 1197−1199.
(13) Jia, Z.; Wang, Z.; Xu, C.; Liang, J.; We, B.; Wu, D.; Zhu, S. *Mater. Sci. Eng. A* **1999**, (271), 395−400.
(14) Gong, X.; Liu, J.; Baskaran, S.; Voise, R. D.; Young, J. S. *Chem. Mater.* **2000**, *12*, 1049−1052.
(15) Jin, Z.; Pramoda, K. P.; Xu, G.; Goh, S. H. *Chem. Phys. Lett.* **2001**, *337*, 43−47.
(16) Safadi, B.; Andrews, R.; Grulke, E. A. *J. Appl. Polym. Sci.* **2002**, *84*, 2660−2669.
(17) Kearns, J. C.; Shambaugh, R. L. *J. Appl. Polym. Sci.* **2002**, *86*, 2079−2084.
(18) Cooper, C. A.; Ravich, D.; Lips, D.; Mayer, J.; Wagner, H. D. *Compos. Sci. Technol.* **2002**, *62*, 1105−1112.
(19) Bower, C.; Rosen, R.; Jin, L.; Han, J.; Zhou, O. *Appl. Phys. Lett.* **1999**, *74*, 3317−3319.
(20) Pötschke, P.; Fornes, T. D.; Paul, D. R. *Polymer* **2002**, *43*, 3247−3255.
(21) Dondero, W. E.; Gorga, R. E. *J. Polym. Sci., Part B: Polym. Phys.* **2006**, *44*, 864−878.
(22) Gorga, R. E.; Cohen, R. E. *J. Polym. Sci., Part B: Polym. Phys.* **2004**, *42*, 2690−2702.
(23) Ponomarenko, A. T.; Shevchenko, V. G.; Enikolopyan, N. S. *Adv. Polym. Sci.* **1990**, *96*, 125−145.
(24) Hooper, J. B.; Schweizer, K. S. *Macromolecules* **2006**, *39*, 5133−5142.
(25) Formhals, A. Process and Apparatus for Preparing Artificial Threads, 1,975,504, 1934.
(26) Li, D.; Xia, Y. *Adv. Mater.* **2004**, *16*, 1151−1170.
(27) Matthews, J. A.; Boland, E. D.; Wnek, G. E.; Simpson, D. G.; Bowlin, G. L. *J. Bioact. Compat. Polym.* **2003**, *18*, 125−134.
(28) Buttafoco, L.; Kolkman, N. G.; Poot, A. A.; Dijkstra, P. J.; Vermes, I.; Feijen, J. *J. Controlled Release* **2005**, *101*, 322−324.
(29) Dror, Y.; Salalha, W.; Khalfin, R. L.; Cohen, Y.; Yarin, A. L.; Zussman, E. *Langmuir* **2003**, *19*, 7012−7020.
(30) Ayutsede, J.; Gandhi, M.; Sukigara, S.; Ye, H. H.; Hsu, C. M.; Gogotsi, Y.; Ko, F. *Biomacromolecules* **2006**, *7*, 208−214.
(31) Ko, F.; Gogotsi, Y.; Ali, A.; Naguib, N.; Ye, H. H.; Yang, G. L.; Li, C.; Willis, P. *Adv. Mater.* **2003**, *15*, 1161−1164.
(32) Mack, J. J.; Viculis, L. M.; Ali, A.; Luoh, R.; Yang, G. L.; Hahn, H. T.; Ko, F. K.; Kaner, R. B. *Adv. Mater.* **2005**, *17*, 77−80.
(33) Sundaray, B.; Subramanian, V.; Natarajan, T. S.; Krishnamurthy, K. *Appl. Phys. Lett.* **2006**, *88*, 143114.
(34) Ren, Z. F.; Huang, Z. P.; Xu, J. W.; Wang, J. K.; Bush, P.; Siegel, M. P.; Provencio, P. *Science* **1998**, *282*, 1105−1107.
(35) Van Gerwen, P.; Laureyn, W.; Laureys, W.; Huyberechts, G.; Op De Beeck, M.; Baert, K.; Suls, J.; Sansen, W.; Jacobs, P.; Hermans, L.; Mertens, R. *Sens. Actuators, B* **1998**, *49*, 73−80.
(36) Brydson, J. *Flow Properties of Polymer Melts*, 1st ed.; Van Nostrand Reinhold: London, 1970.
(37) Stauffer, D.; Aharony, A. *Introduction to Percolation Theory*, 2nd ed.; Taylor & Francis: Washington, DC, 1992.
(38) Cheah, K.; Simon, G. P.; Forsyth, M. *Polym. Int.* **2001**, *50*, 27−36.
(39) Mamunya, E. P.; Davidenko, V. V.; Lebedev, E. V. *Polym. Compos.* **1995**, *16*, 319−324.
(40) Rahatekar, S. S.; Hamm, M.; Shaffer, M. S. P.; Eliott, J. A. *J. Chem. Phys.* **2005**, *123*, 134702.
(41) Balberg, I.; Binenbaum, N.; Wagner, N. *Phys. Rev. Lett.* **1984**, *52*, 1465−1468.
(42) Du, F.; Fischer, J. E.; Winey, K. I. *Phys. Rev. B* **2005**, *72*, 121404-(R).
(43) Grujicic, M.; Cao, G.; Roy, W. N. *J. Mater. Sci.* **2004**, *39*, 4441−4449.
(44) Natsuki, T.; Endo, M.; Takahashi, T. *Physica A* **2005**, *352*, 498−508.
(45) Ueda, N.; Taya, M. *J. Appl. Phys.* **1986**, *60*, 459−461.
(46) Hobbie, E. K.; Obrzut, J.; Kharchenko, S. B.; Grulke, E. A. *J. Chem. Phys.* **2006**, *125*, 044712.
(47) McLachlan, D. S. *J. Electroceram.* **2000**, *5*, 93−110.
(48) Cheah, K.; Forsyth, M.; Simon, G. P. *J. Polym. Sci., Part B: Polym. Phys.* **2000**, *38*, 3106−3119.
(49) Huang, J.-C. *Adv. Polym. Technol.* **2002**, *21*, 299−313.
(50) Thongruang, W.; Balik, C. M.; Spontak, R. J. *J. Polym. Sci., Part B: Polym. Phys.* **2002**, *40*, 1013−1023.
(51) Thongruang, W.; Spontak, R. J.; Balik, C. M. *Polymer* **2002**, *43*, 3717−3725.
(52) Fournier, J.; Boiteux, G.; Seytre, G.; Marichy, G. *Synth. Met.* **1997**, *84*, 839−840.
(53) Coleman, J. N.; Curran, S.; Dalton, A. B.; Davey, A. P.; McCarthy, B.; Blau, W.; Barklie, R. C. *Phys. Rev. B* **1998**, *58*, R7492−7495.
(54) Vionnet-Menot, S.; Grimaldi, C.; Maeder, T.; Strässler, S.; Ryser, P. *Phys. Rev. B* **2005**, *71*, 064201.
(55) Frank, D. J.; Lobb, C. *J. Phys. Rev. B* **1988**, *37*, 302−307.
(56) Smith, L. N.; Lobb, C. J. *Phys. Rev. B* **1979**, *20*, 3653−3658.
(57) Gubbels, F.; Jerómé, R.; Teyssié, P.; Vanlathem, E.; Deltour, R.; Calderone, A.; Parenta, V.; Brédas, J. L. *Macromolecules* **1994**, *27*, 1972−1974.
(58) Kilbride, B. E.; Coleman, J. N.; Fraysse, J.; Fournet, P.; Cadek, M.; Drury, A.; Hutzler, S.; Roth, S.; Blau, W. J. J. *J. Appl. Phys.* **2002**, *92*, 4024−30.
(59) Barrau, S.; Demont, P.; Peigney, A.; Laurent, C. C. L. *Macromolecules* **2003**, *36*, 5187−5194.
(60) McLachlan, D. S.; Chiteme, C.; Park, C.; Wise, K. E.; Lowther, S. E.; Lillehei, P. T.; Siochi, E. J.; Harrison, J. S. *J. Polym. Sci., Part B: Polym. Phys.* **2005**, *43*, 3273−3287.
(61) Calberg, C.; Blacher, S.; Gubbels, F.; Brouers, F.; Deltour, R.; Jerómé, R. *J. Phys. D: Appl. Phys.* **1999**, *32*, 1517−1525.
(62) Wan, Y.; Fang, Y.; Hu, Z.; Wu, Q. *Macromol. Rapid Commun.* **2006**, *27*, 948−954.
(63) The small number of points below threshold lend less reliability to the *s* value compared with our estimate of *t*.
(64) Dalmas, F.; Dendievel, R.; Chazeau, L.; Cavaillé, J.-Y.; Gauthier, C. *Acta Material.* **2006**, *54*, 2923−2931.

MA061735C